Sea ice floe impact experiments

Frederking, Robert; Timco, Garry; Reid, Scott

Publisher's version / Version de l'éditeur:
https://doi.org/10.4224/12340959
PERD/CHC Report; no. 8-96, 1999-03

CHC CANADIAN HYDRAULICS CENTRE

Sea Ice Floe Impact Experiments

R. Frederking, G.W. Timco & S. Reid
Canadian Hydraulics Centre
National Research Council of Canada
Ottawa, Ont. K1A 0R6
Canada

Technical Report
HYD-TR-038
PERD/CHC Report 8-96

March 1999

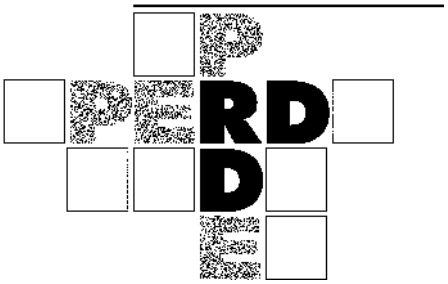

ABSTRACT

The impact of ice floes can be an important part of the design considerations for structures placed offshore in Eastern Canada. A laboratory test program has been performed to investigate the force levels due to the impact of an isolated floe with a structure. In these tests, large floes of sea ice (up to 14 tonnes) were grown in an ice tank, and they were accelerated to impact an instrumented test structure. The load level and local pressure during the impact were measured. Fifty-two impact tests were conducted. The maximum load was a function of the shape of the impact interface. The highest load levels measured were on the order of 50 kN for ice floes with speeds of 0.2 m/s. This report presents a full description of the test procedures and provides the results of the tests.

TABLE OF CONTENTS

LIST OF FIGURES

LIST OF TABLES

Sea Ice Floe Impact Experiments

1. INTRODUCTION

Offshore structures that are placed in ice-covered waters have to be designed to withstand the forces generated by the ice. In severe ice environments, such as the Beaufort Sea or the Hibernia location, the interaction with large, extreme ice features dominates the structural design. Considerable effort has been spent in developing an understanding of the interaction of these large ice features with a structure. In some offshore regions of Canada, such as the Sable Island area, ice is present on a limited basis. Moreover, in parts of the Grand Banks regions of Canada, floating pack ice can be present for several weeks of the year (Wright et al. 1998). In these regions, the ice forces on any fixed or floating offshore structure would be generated by the interaction of loose ice floes colliding with the structure. For this type of interaction, little quantitative information is available to predict the ice loads.

Some work has been done to measure impact forces on bridge piers (Haynes et al. 1991; Frederking and Sayed, 1989). In these studies, individual bridge piers have been instrumented to measure forces from the collision of single ice floes during the spring break-up of the river ice. Information is available on the ice forces, but limited information is available on the floe size and speed; hence, estimates of the kinetic energy and impact force cannot be obtained and extrapolation of the data to other ice regimes is not possible.

This report provides information on a controlled laboratory experiment to measure the forces of a sea ice floe colliding with a fixed structure. Large floes of saline ice were grown in an ice tank and they were pushed such as to float into and collide with an instrumented structure. The full details of the experiments are described and the results are presented for all tests.

2. EXPERIMENTAL ARRANGEMENT

The tests were carried out in the ice tank in a large environmental test chamber at the Canadian Hydraulics Centre at NRC. The temperature in the chamber can be maintained at a pre-selected value within the range –20°C to +20°C. The chamber is 29 meters long, 10 meters wide and 4.9 meters high. It houses a 21 m long by 7 m wide by 1.2 m deep ice tank (Pratte and Timco, 1981). Because the volume of the tank is relatively small, it is possible to change the water in the tank and grow ice from various solutions. Normally EG/AD/S model ice is grown in the tank for reduced scale tests of ice covers interacting with structures. In the case of this test program, the objective was to study impact forces of ice floes having the same properties as sea ice in nature. The two main factors affecting sea ice strength are temperature and salinity. Sea ice has a salinity of about 5 $^{o}/_{oo}$ (parts per thousand), so this was the target for this test program. Ice salinity is a function of the original seawater salinity and the growth rate. Because ice growth in the chamber would be faster than in nature, a reduced salinity solution was used, 16 $^{o}/_{oo}$ as compared to 32 $^{o}/_{oo}$ for natural seawater.

Testing required a free floating ice sheet to impact against an instrumented structure. Therefore one of the requirements in setting up the test conditions was ensuring a free floating ice sheet. One approach would have been to grow an ice sheet and then cut it free from the walls of the tank. This would have required a great deal of labour to cut and remove the excess ice. The approach used here was to surround the floe area with sheets of foam insulation to prevent ice formation in the first place. The arrangement was supplemented by immersible heat tapes placed just under the insulation. The layout of the ice tank with insulation and structure placement is shown in Figure 1. The insulation and heating tapes were removed at the start of the testing.

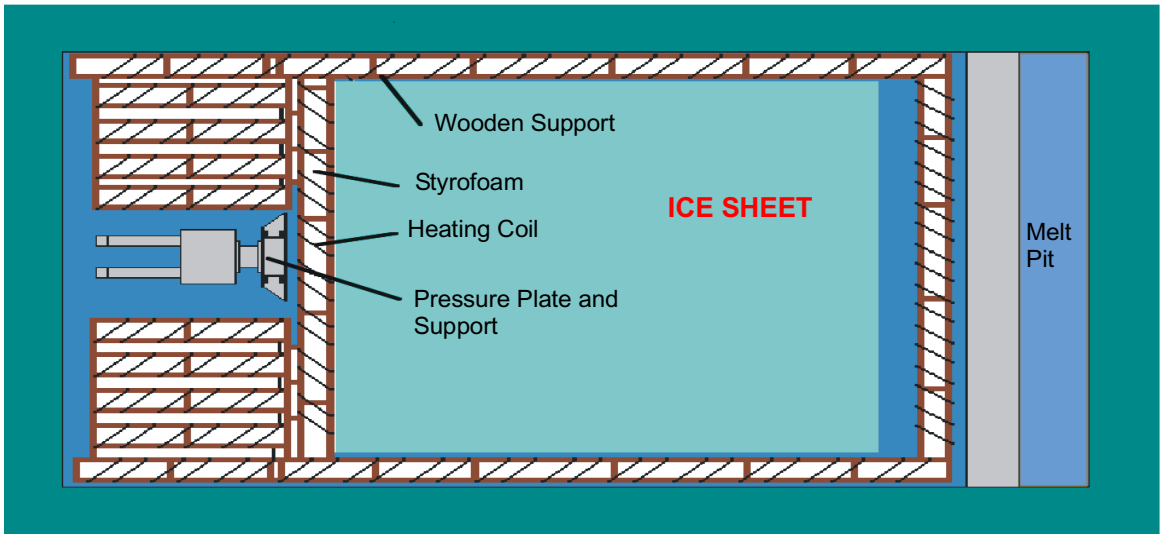

Figure 1 General arrangement in the ice tank for growing the ice sheet.

The instrumented test structure was attached to a stand that was anchored to the bottom of one end of the ice tank. A 45 kN capacity six-component dynamometer (Advanced Mechanical Technology Inc. SRMC8-X-10000) was placed between the test structure and the stand to measure force components in the longitudinal, transverse and vertical directions. The general arrangement is shown in Figure 2.

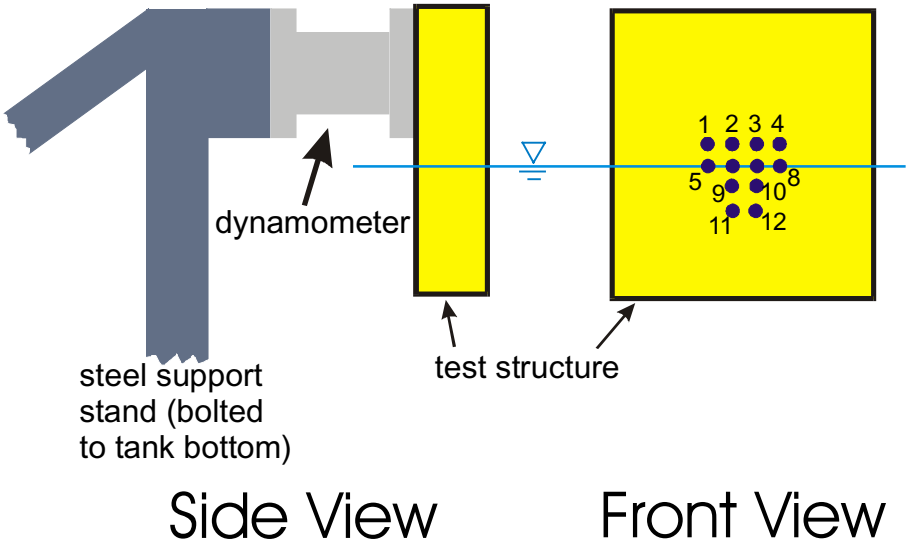

Figure 2 Test stand and structure arrangement.

The test structure was a 12.7 mm thick framed plate that bolted to the front face of the dynamometer. The plate was 508 mm wide by 584 mm high. A drawing of the test structure is shown in Figure 3. An array of 12 local pressure sensors was placed in the front face of the test structure to provide an indication of contact area, pressure distribution and magnitude of local pressures. The sensors were spaced 50.4 mm on centre and distributed on the front face of the test structure as shown in Figure 2. A schematic of the one of the local pressure sensors is shown in Figure 4. The total ice load transmitted to the sensor's 12.7 mm diameter moveable piston is measured with a miniature load cell. The sensors have a capacity of 70 MPa.

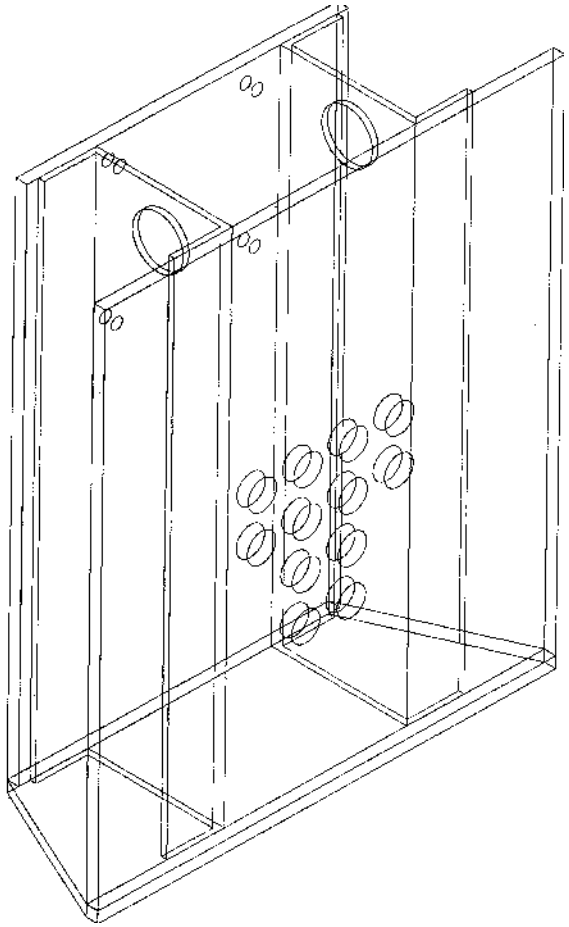

Figure 3 Schematic of test structure.

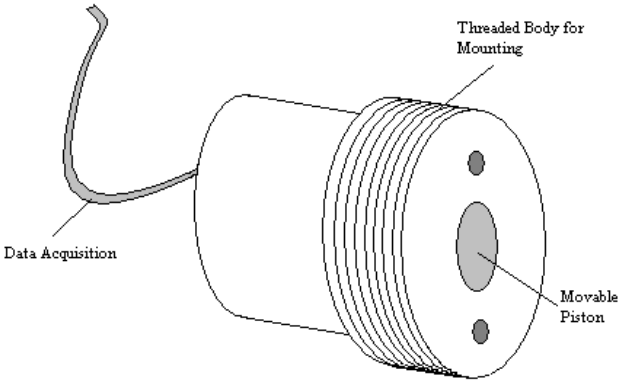

Figure 4 Local pressure sensors.

Additional instrumentation consisted of three accelerometers, one placed on top of the test structure, and two at the centre of the ice floe oriented in the longitudinal and transverse directions. A video camera was used to film a side view of each impact. Figure 5 shows an overview of the test arrangement in the ice tank.

The test results were recorded using CHC's in-house data acquisition program, GEDAP. It is a general-purpose software system for the acquisition, analysis and management of laboratory data. The analogue signals from the dynamometer, pressure sensors and accelerometers were digitized and recorded at 1000 Hz per channel.

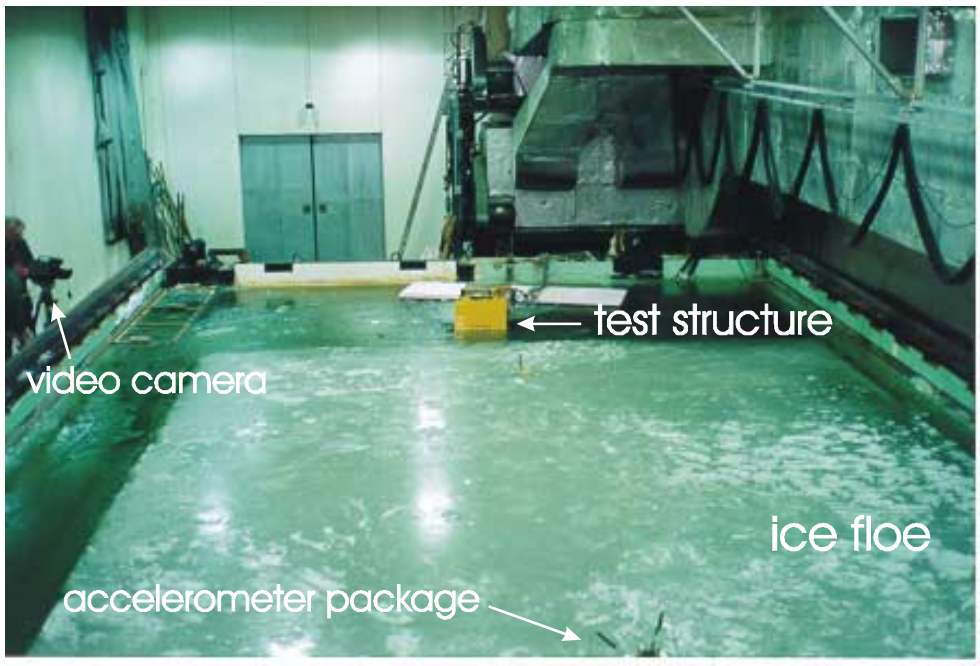

Figure 5 Overview of the ice floe in the ice tank showing the test structure, video camera and accelerometer package on the ice floe.

3. TEST PROCEDURE AND MEASUREMENTS

Ice growth started on April 3 and reached a thickness of 215 mm by April 14. The ice sheet was allowed to grow naturally and there was no initial (seeding) nucleation. Air temperature during the growth period varied from –10°C to –15°C. The ice floe was about 11.9 m long by 5.75 m wide.

Tests were run using the towing carriage in the tank to accelerate the ice floe to a known speed, and then letting it drift under its own momentum into the test structure. The test variables included impact speed, shape of the ice edge contacting the test structure and mass of the ice floe. Eight different ice edge shapes were made as illustrated in Figure 6.[1] An example of the 90° wedge-shaped edge impacting the test structure is shown in Figure 7. Care was taken to ensure that the ice edge impacted the centre of the test structure. In some cases, a reach pole was used to provide lateral guidance to the ice sheet. This was done in a manner so as not to influence the impact velocity of the ice sheet. A total of 52 impact tests was conducted, 2 on April 14, 19 on April 15 and 31 on April 15. The test conditions are outlined in Table 1. Following each test, visual observations were made of the impact zone (see Figure 8). The velocities listed in Table 1 represent the velocity of the carriage at the time the ice floe was "released" for impact.

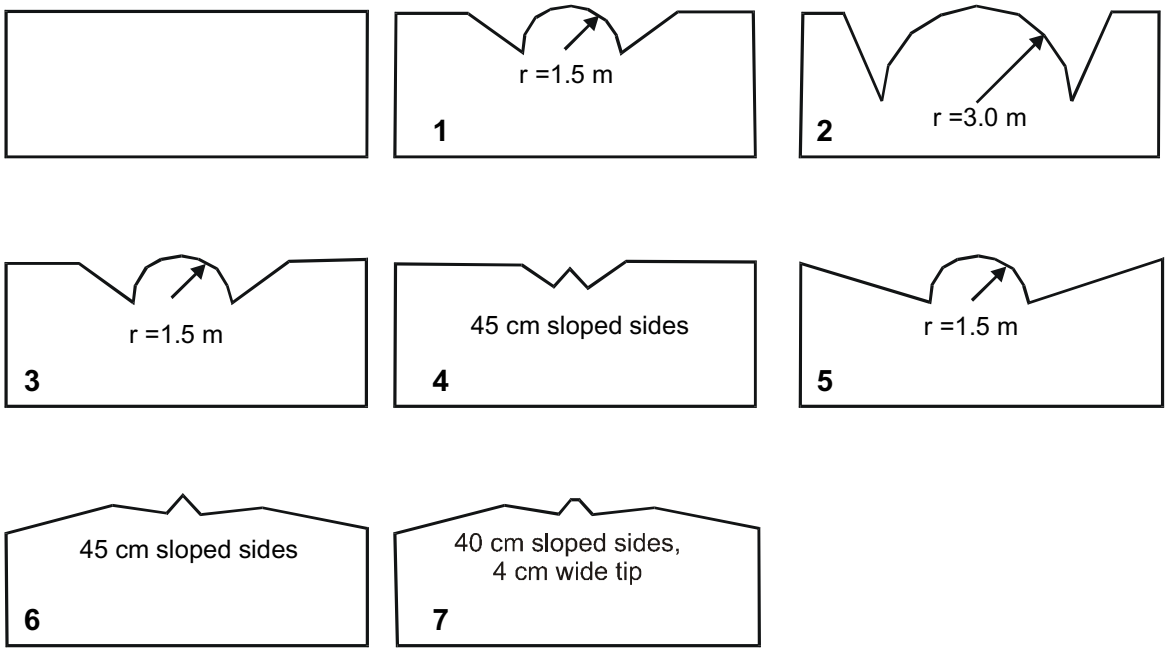

Figure 6 Geometry of ice edges used in tests.

[1] Note that while Edges 1 and 3 (Figure 6) are the same, Edge 3 was freshly cut from Edge 2 after 3 tests were conducted on it.

Figure 7 Floe with 90° wedge-shaped edge (#4) impacting test structure

Figure 8 Measurement of the impact zone following a test.

Table 1 Test Conditions

Test Number	Test Date	Nominal Velocity of Ice Floe from carriage speed (mm/s)	Ice Floe Size (length x width x thickness)	Calculated Ice Floe Mass (tonnes)	Ice Floe Edge (see Figure 6)
Test 1	14/Apr	unknown	11.9m x 5.75m x 216mm	13.7	Straight Edge
Test 2	14/Apr	unknown	11.9m x 5.75m x 216mm	13.7	Straight Edge
Test 3	15/Apr	50	11.9m x 5.75m x 225mm	14.3	Straight Edge
Test 4	15/Apr	80	11.9m x 5.75m x 225mm	14.3	Straight Edge
Test 5	15/Apr	150	11.9m x 5.75m x 225mm	14.3	Straight Edge
Test 6	15/Apr	200	11.9m x 5.75m x 225mm	14.3	Straight Edge
Test 7	15/Apr	50	11.9m x 5.75m x 225mm	14.3	Shaped Edge #1
Test 8	15/Apr	80	11.9m x 5.75m x 225mm	14.3	Shaped Edge #1
Test 9	15/Apr	150	11.9m x 5.75m x 225mm	14.3	Shaped Edge #1
Test 10	15/Apr	200	11.9m x 5.75m x 225mm	14.3	Shaped Edge #1
Test 11	15/Apr	200	11.9m x 5.75m x 225mm	14.3	Shaped Edge #1
Test 12	15/Apr	20	11.9m x 5.75m x 225mm	14.3	Shaped Edge #2
Test 13	15/Apr	50	11.9m x 5.75m x 225mm	14.3	Shaped Edge #2
Test 14	15/Apr	50	11.9m x 5.75m x 225mm	14.3	Shaped Edge #2
Test 15	15/Apr	30	11.9m x 5.75m x 225mm	14.3	Shaped Edge #3
Test 16	15/Apr	50	11.9m x 5.75m x 225mm	14.3	Shaped Edge #3
Test 17	15/Apr	50	11.9m x 5.75m x 225mm	14.3	Shaped Edge #3
Test 18	15/Apr	30	11.9m x 5.75m x 225mm	14.3	Shaped Edge #4
Test 19	15/Apr	50	11.9m x 5.75m x 225mm	14.3	Shaped Edge #4
Test 20	15/Apr	70	11.9m x 5.75m x 225mm	14.3	Shaped Edge #4
Test 21	15/Apr	70	11.9m x 5.75m x 225mm	14.3	Shaped Edge #4
Test 22	16/Apr	30	6.5m x 5.75m x 235mm	7.8	Shaped Edge #5
Test 23	16/Apr	50	6.5m x 5.75m x 235mm	7.8	Shaped Edge #5
Test 24	16/Apr	50	6.5m x 5.75m x 235mm	7.8	Shaped Edge #5
Test 25	16/Apr	60	6.5m x 5.75m x 235mm	7.8	Shaped Edge #5
Test 26	16/Apr	70	6.5m x 5.75m x 235mm	7.8	Shaped Edge #5
Test 27	16/Apr	70	6.5m x 5.75m x 235mm	7.8	Shaped Edge #5
Test 28	16/Apr	30	6.5m x 5.75m x 235mm	7.8	Shaped Edge #6
Test 29	16/Apr	50	6.5m x 5.75m x 235mm	7.8	Shaped Edge #6
Test 30	16/Apr	70	6.5m x 5.75m x 235mm	7.8	Shaped Edge #6
Test 31	16/Apr	80	6.5m x 5.75m x 235mm	7.8	Shaped Edge #6
Test 32	16/Apr	90	6.5m x 5.75m x 235mm	7.8	Shaped Edge #6
Test 33	16/Apr	90	6.5m x 5.75m x 235mm	7.8	Shaped Edge #6
Test 34	16/Apr	90	6.5m x 5.75m x 235mm	7.8	Shaped Edge #6
Test 35	16/Apr	100	6.5m x 5.75m x 235mm	7.8	Shaped Edge #6
Test 36	16/Apr	100	6.5m x 5.75m x 235mm	7.8	Shaped Edge #6
Test 37	16/Apr	100	6.5m x 5.75m x 235mm	7.8	Shaped Edge #6
Test 38	16/Apr	120	6.5m x 5.75m x 235mm	7.8	Shaped Edge #6
Test 39	16/Apr	120	6.5m x 5.75m x 235mm	7.8	Shaped Edge #6
Test 40	16/Apr	120	6.5m x 5.75m x 235mm	7.8	Shaped Edge #6
Test 41	16/Apr	120	6.5m x 5.75m x 235mm	7.8	Shaped Edge #6
Test 42	16/Apr	50	3.5m x 5.75m x 220mm	4.1	Shaped Edge #6
Test 43	16/Apr	50	3.5m x 5.75m x 220mm	4.1	Shaped Edge #6
Test 44	16/Apr	70	3.5m x 5.75m x 220mm	4.1	Shaped Edge #6
Test 45	16/Apr	70	3.5m x 5.75m x 220mm	4.1	Shaped Edge #6
Test 46	16/Apr	100	3.5m x 5.75m x 220mm	4.1	Shaped Edge #6
Test 47	16/Apr	100	3.5m x 5.75m x 220mm	4.1	Shaped Edge #6
Test 48	16/Apr	140	3.5m x 5.75m x 220mm	4.1	Shaped Edge #6
Test 49	16/Apr	140	3.5m x 5.75m x 220mm	4.1	Shaped Edge #6
Test 50	16/Apr	50	3.5m x 5.75m x 220mm	4.1	Shaped Edge #7
Test 51	16/Apr	70	3.5m x 5.75m x 220mm	4.1	Shaped Edge #7
Test 52	16/Apr	100	3.5m x 5.75m x 220mm	4.1	Shaped Edge #7

From Table 1 it can be seen that there was a slight increase in ice thickness from April 14 to April 16. Density of the ice sheet was determined by a measure of the ice sheet thickness and its freeboard. On April 14 the thickness and freeboard were 216 mm and 20 mm respectively. Using these measures and a density of 1015 kg/m^3 for sea water of 16 $^{o}/_{oo}$ salinity, a bulk density of 920 kg/m^3 was obtained for the ice sheet. Thickness and freeboard measurements on April 15 were 225 mm and 17 mm respectively giving a density of 940 kg/m^3. A value of 930 kg/m^3 was used for calculating the mass of the ice sheets in Table 1. Samples of the ice sheets were taken on April 15 and April 16 for salinity measurements. The salinity profiles are plotted in Figure 9.

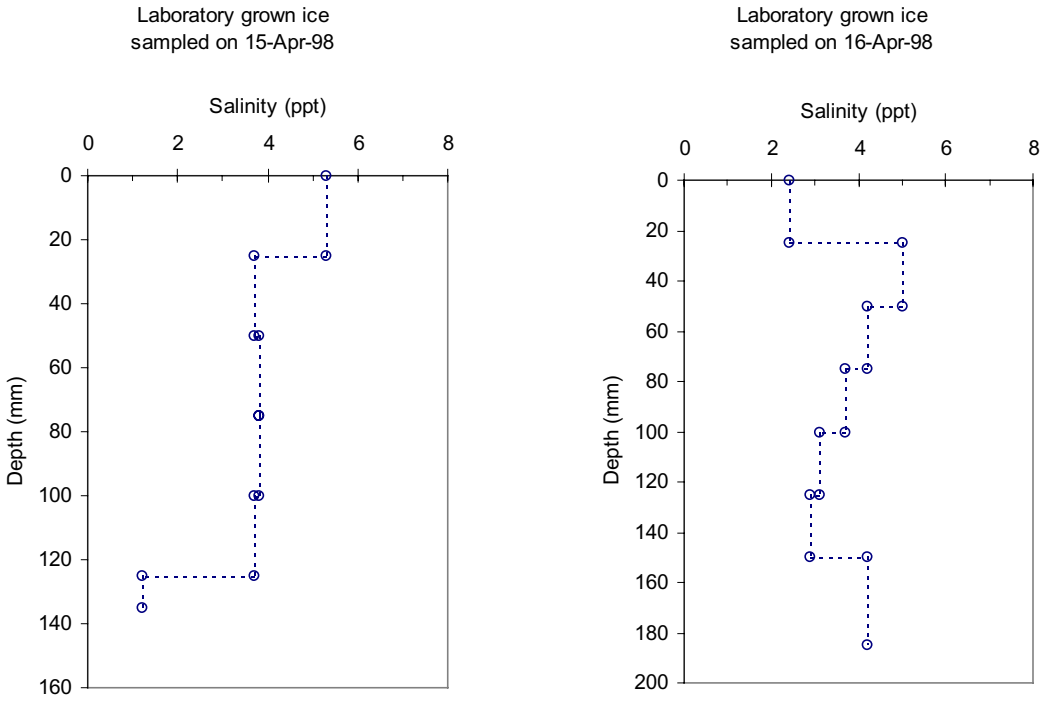

Figure 9 Salinity profiles of ice sheet samples taken on April 15 and 16

The microstructure of ice from the 15 and 16 April ice impact tests was examined. Vertical and horizontal thin sections of ice were prepared using the hot-plate technique. A polariscope was used to examine the thin sections of ice under both crossed polarized and plane polarized light.

Figure 10(a) shows the vertical thin section (extending from 0 - 140 mm) for the 15 April ice. The top 30 mm of ice is comprised of a translucent white layer of ice, that contains air inclusions that are about 2 mm in diameter. Below a depth of about 30 mm, columnar grains of ice form and their diameters increase in size with increasing depth. To highlight the presence of inclusions, the vertical thin section was examined under parallel polarized light (not shown), which showed that a considerable amount of air was entrained in the ice during the growth process.

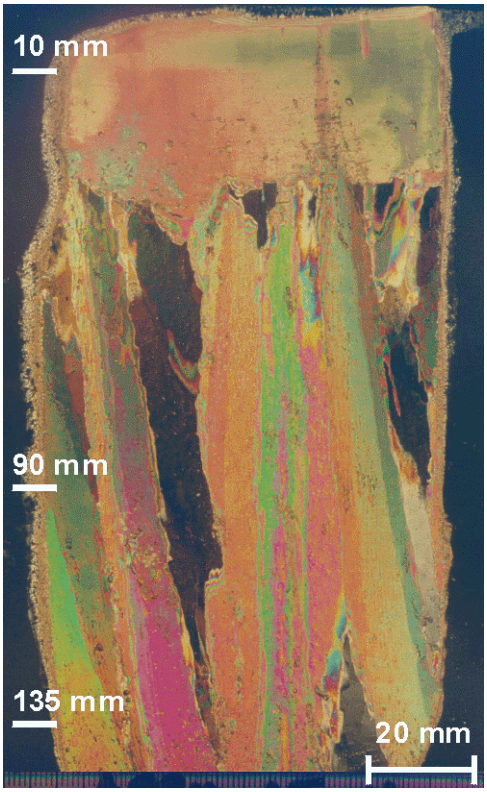

(a) 15 April ice: vertical section

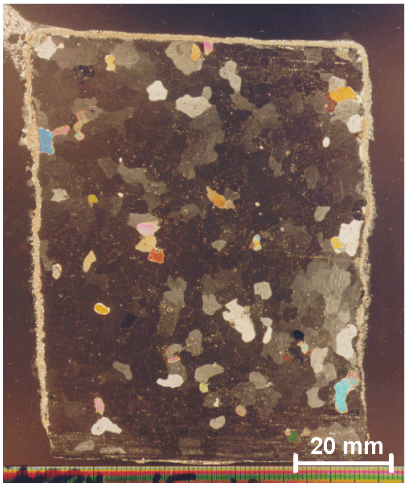

(b) horizontal section at 10 mm

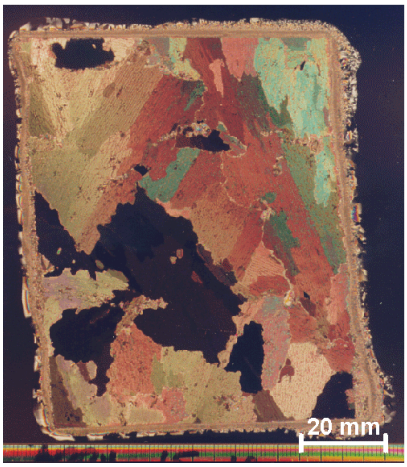

(c) horizontal section at 90 mm

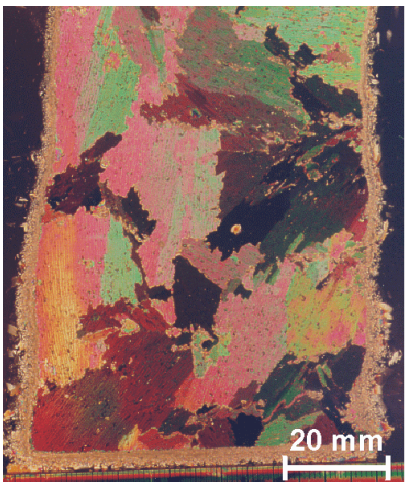

(d) horizontal section at 135 mm

Figure 10 Thin sections of ice sampled on April 15

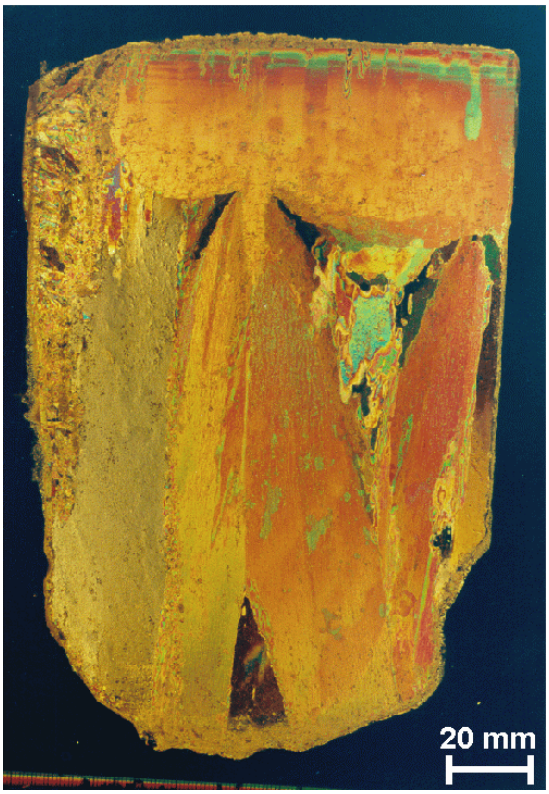

(a) 16 April ice: vertical section

(b) 16 April ice: vertical section showing impacted face

Figure 11 Thin sections of ice sampled on April 16

A horizontal thin section from a depth of 10 mm in Figure 10(b) was prepared from the surface layer of ice. What appeared to be a large, single crystal of ice in the surface layer of the vertical section, actually consisted of fine (about 5 mm) grain material. Figure 10(b) shows that the c-axis of most of the grains is in the extinct position, which indicates vertically aligned c-axis of the grains. The surface layer of ice is classified as **P1**, or primary ice with a vertically oriented c-axis.

Figure 10(c) and (d) show horizontal sections from depths of 90 mm and 135 mm that were prepared from the columnar zone. The grains in the section from 90 mm have a grain size of the order of 10 mm, which increases to 25 mm wide at 135 mm depth. Both sections from the columnar zone show a distinct sub-granular structure. The distance between adjacent rows of brine, or brine layer spacing, decreases from 0.5 mm at a depth of 90 mm to slightly less at a depth of 135 mm. The orientation of the c-axis (in the horizontal plane) can be inferred from the arrangement of the rows of brine. The sections do not show any preferred alignment of the c-axis of the grains. As such, the ice is classified as columnar ice with a random, horizontal c-axis (**S2** type ice after Michel and Ramseier, 1971).

Figure 11(a) presents a vertical thin section that was prepared from the 16 April ice. From the appearance of grain boundaries, it shows larger and more angled grains than the 15 April ice. Both of these factors could indicate a heightened competition for growth between adjacent grains. After the 16 April ice impact tests, an ice block was removed from the impacted area of the ice sheet and a vertical thin section was prepared (Figure 11(b)). Examination of the section with the aid of a polariscope and crossed polarized light did not reveal any macro-or micro-cracks in the thin section. The thin sections were made some time after the testing, so if cracks were initially present there was time for them to heal.

4. RESULTS

The analysis results of impact velocity and duration, floe mass, and maximum values of force and acceleration are presented in Table 2. The values of mass differ from those in Table 1 because in this case, it is determined from the relation between the maximum impact force and maximum impact acceleration for each floe size (see Section 4.2 and Figure 19). The maximum values of force and acceleration are derived from the time series traces in Appendix A. In the cases of tests 7, 8, 9 and 10, the dynamometer was overloaded, so in these tests the maximum force was inferred from the maximum acceleration and the floe mass. These values of force are indicated in bold italics in Table 2. Measured impact velocity is different from the velocity in Table 1 because in this case it was determined from analysis of the video records. Time to traverse a distance of 274 mm was determined to within ± 0.1 s. Thus the uncertainty at velocities of about 100 mm/s was ± 4 mm/s. At 200 mm/s the uncertainty increased to ± 15 mm/s and at a lower velocity of 20 mm/s, the uncertainty decreased to ± 0.2 mm/s. Plots of time series of resultant force on the test structure measured by the dynamometer, deceleration of the floe in the x-direction (as measured with the accelerometer), and pressures measured by the pressure sensors are presented for each test in Appendix A. To illustrate the results in Appendix A, one test, Test 20, will be presented and discussed in detail in Section 4.1.

Table 2 Test Results

Test Number	Ice Floe Edge Shape (see Figure 6)	Edge Thickness (mm)	Measured Velocity (mm/s)	Ice Floe Mass (tonnes)	Maximum Force (kN)	Maximum Acceleration (m/s^2)	Impact Duration (s)
Test 1	Straight Edge	-	86	11.5	10.9	0.93	0.22
Test 2	Straight Edge	-	150	11.5	10.6	0.92	0.375
Test 3	Straight Edge	115	61	13.0	1.12	0.06	1.55
Test 4	Straight Edge	115	97	13.0	9.3	0.82	0.33
Test 5	Straight Edge	115	129	13.0	15.8	1.41	0.31
Test 6	Straight Edge	115	234	13.0	24.2	1.98	0.32
Test 7	Shaped Edge #1	115	52	13.0	***7.2***	0.63	0.24
Test 8	Shaped Edge #1	115	109	13.0	***8.3***	0.63	0.30
Test 9	Shaped Edge #1	115	141	13.0	***46.8***	3.60	0.18
Test 10	Shaped Edge #1	115	194	13.0	***48.7***	3.75	0.15
Test 11	Shaped Edge #1	115	169	13.0	***39.7***	3.06	0.20
Test 12	Shaped Edge #2	137	23	13.0	0.24	0.00	1.25
Test 13	Shaped Edge #2	137	61	13.0	11.0	0.96	0.18
Test 14	Shaped Edge #2	137	57	13.0	7.6	0.62	0.18
Test 15	Shaped Edge #3	137	33	13.0	1.5	0.12	0.6
Test 16	Shaped Edge #3	137	64	13.0	12.8	1.03	0.21
Test 17	Shaped Edge #3	137	45	13.0	12.5	1.03	0.21
Test 18	Shaped Edge #4	150	42	13.0	5.35	0.41	0.24
Test 19	Shaped Edge #4	150	57	13.0	5.73	0.46	0.35
Test 20	Shaped Edge #4	150	114	13.0	6.60	0.52	0.42
Test 21	Shaped Edge #4	150	106	13.0	8.19	0.67	0.35
Test 22	Shaped Edge #5	180	30	6.8	0.35	0.07	1.20
Test 23	Shaped Edge #5	180	46	6.8	4.94	0.69	0.20
Test 24	Shaped Edge #5	180	47	6.8	4.55	0.62	0.17
Test 25	Shaped Edge #5	180	58	6.8	5.88	0.83	0.17
Test 26	Shaped Edge #5	180	94	6.8	12.3	1.78	0.17
Test 27	Shaped Edge #5	180	70	6.8	9.48	1.31	0.15
Test 28	Shaped Edge #6	185	28	6.8	2.84	0.40	0.20
Test 29	Shaped Edge #6	185	53	6.8	2.86	0.41	0.28
Test 30	Shaped Edge #6	185	66	6.8	5.51	0.81	0.19
Test 31	Shaped Edge #6	185	70	6.8	5.47	0.78	0.19
Test 32	Shaped Edge #6	185	76	6.8	7.99	1.14	0.17
Test 33	Shaped Edge #6	185	85	6.8	8.36	1.20	0.16
Test 34	Shaped Edge #6	185	79	6.8	8.46	1.26	0.15
Test 35	Shaped Edge #6	185	93	6.8	8.55	1.29	0.21
Test 36	Shaped Edge #6	185	101	6.8	9.14	1.33	0.17
Test 37	Shaped Edge #6	185	115	6.8	12.4	1.93	0.18
Test 38	Shaped Edge #6	185	111	6.8	13.5	1.94	0.15
Test 39	Shaped Edge #6	185	133	6.8	13.3	1.89	0.17
Test 40	Shaped Edge #6	185	100	6.8	11.9	1.74	0.15
Test 41	Shaped Edge #6	185	121	6.8	12.2	1.82	0.17
Test 42	Shaped Edge #6	185	55	3.4	4.02	1.21	0.11
Test 43	Shaped Edge #6	185	56	3.4	4.12	1.17	0.105
Test 44	Shaped Edge #6	185	70	3.4	4.80	1.36	0.12
Test 45	Shaped Edge #6	185	80	3.4	4.79	1.42	0.17
Test 46	Shaped Edge #6	185	113	3.4	7.87	2.39	0.12
Test 47	Shaped Edge #6	185	93	3.4	6.56	1.96	0.125
Test 48	Shaped Edge #6	185	163	3.4	10.6	3.15	0.105
Test 49	Shaped Edge #6	185	164	3.4	15.0	4.38	0.10
Test 50	Shaped Edge #7	185	47	3.4	1.66	0.53	0.52
Test 51	Shaped Edge #7	185	69	3.4	5.49	1.61	0.15
Test 52	Shaped Edge #7	185	95	3.4	8.87	2.65	0.11

4.1. Test 20

Test 20 was an impact of a 14.3 tonne floe with a 90° wedge edge at a velocity of 114 mm/s. By going through the results of this test, the data in the appendices and subsequent analysis will be clearer. The first record to examine is of the two force components in the x- and y-directions (see Figure 12). The force in the x-direction is the predominant force, with very little force in the y-direction, as was the case in all tests. Note that the increase of force was not smooth; that is, there were local failures of the ice that resulted in a saw-tooth characteristic in the force-time record. Viewing the video record showed visible crushing failure of the leading edge of the ice. Some of the tests had this sort of a time series record while others had a smoother sinusoidal shape. The forces in the x-and y-direction were combined to obtain a resultant force.

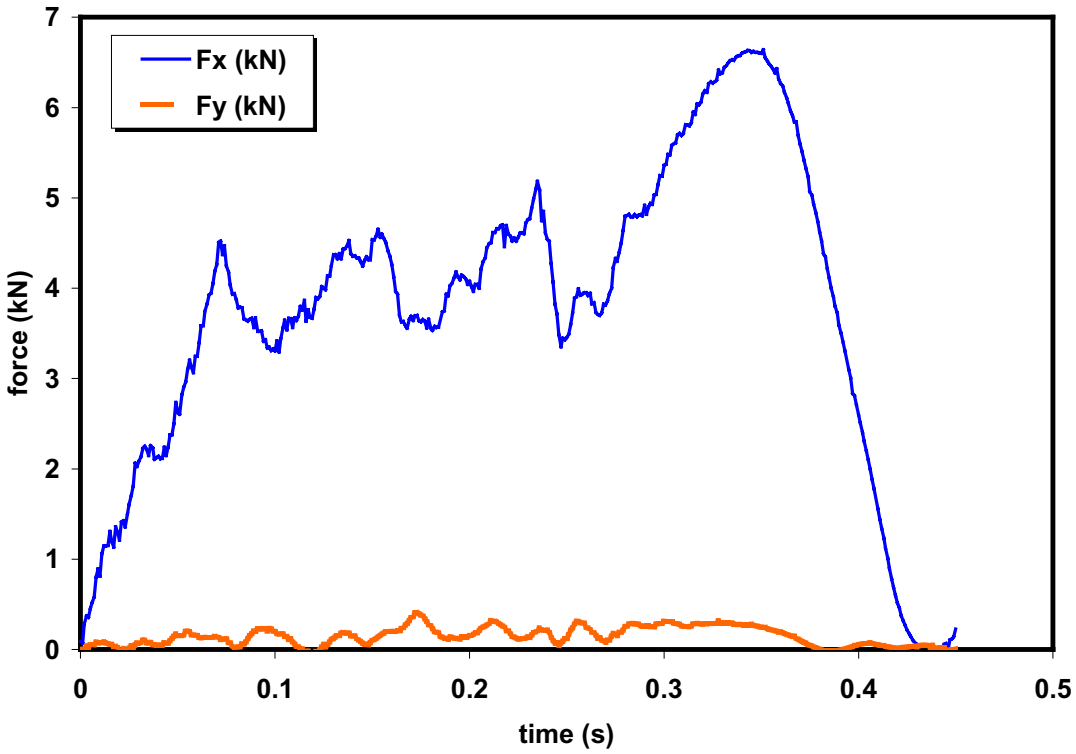

Figure 12 Dynamometer forces in x- and y-directions for Test 20

The other fundamental parameter that was measured was the deceleration (negative acceleration) of the floe. Figure 13 is a plot of acceleration versus time. In this instance the acceleration has a large high frequency component at a frequency of about 100 Hz. The accelerometer was located at the centre of the 12-m long floe. Taking a time of 0.01 s for a compression wave to travel from the centre of the floe to one end and back again, this would correspond to an acoustic velocity of about 1200 m/s. An elastic modulus of about 1 to 1.5 GPa, a reasonable value for warm sea ice, would give this

value of acoustic velocity. Because of the high frequency component in the acceleration, a moving average technique was applied to obtain a "smoothed" acceleration. This smoother acceleration mirrors the measured force of Figure 12. Also shown on Figure 13 is a velocity calculated from the acceleration, starting with an initial impact velocity of 114 mm/s. The time to zero velocity is a bit shorter than the time to zero acceleration, implying that the calculated impact velocity was a bit too small. Integrating the velocity gave a penetration of about 25 mm, a value that corresponds to that observed in the video.

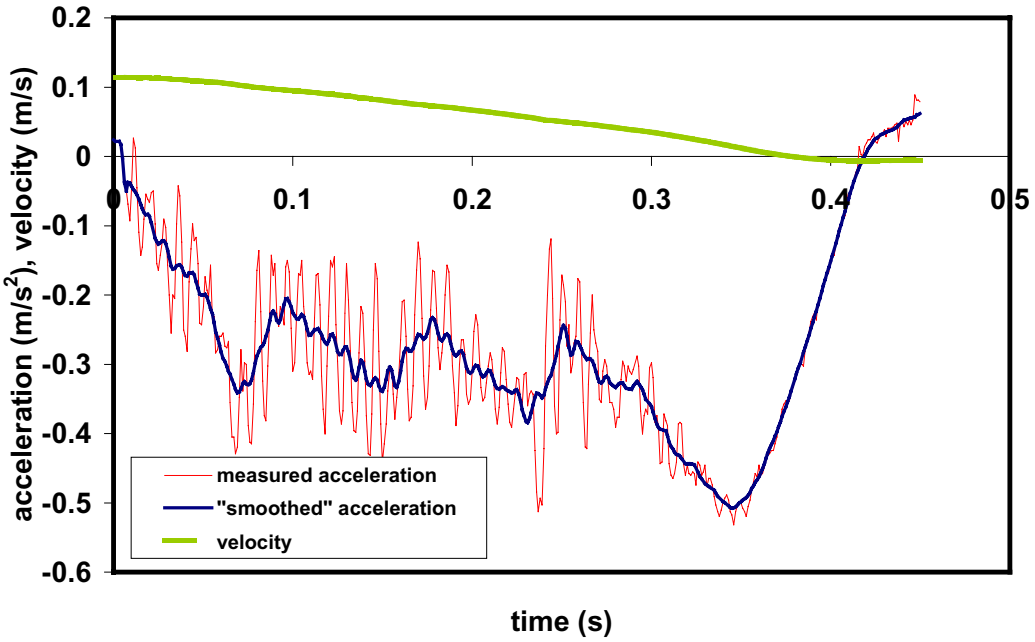

Figure 13 Acceleration (m/s^2) and velocity (m/s) as a function of time in Test 20

Another quantity that can be calculated is the inferred total "mass" of the ice floe, including the added mass of entrained water with the floe. This was done by dividing the measured force by the floe acceleration. The result of this calculation is plotted in Figure 14. Ignoring the start and end of the impact, where one is dividing by a small value of acceleration, a reasonably consistent value of "mass" is obtained. In this case the "smoothed" acceleration was used in the calculation, but since only an average value is being sought, no error is introduced. The calculated "mass" was 13.9 tonnes as compared to 14.3 tonnes (Table 1) estimated from measurements of floe geometry and density. The "added mass" due to entrained water moving with the floe is included in the "mass" value. While not explored in this report, the data could be used to determine such added mass effects for ice floes having geometries similar to those used in this test program. It is also possible to use calculated "mass" to determine an "equivalent" force; i.e., "mass" times acceleration. Figure 15 compares the dynamometer measured force F_x from Figure 12 and the calculated or "inferred" total force "F_{xi}". It can be seen that, taking the high frequency component of acceleration out, the two forces agree closely.

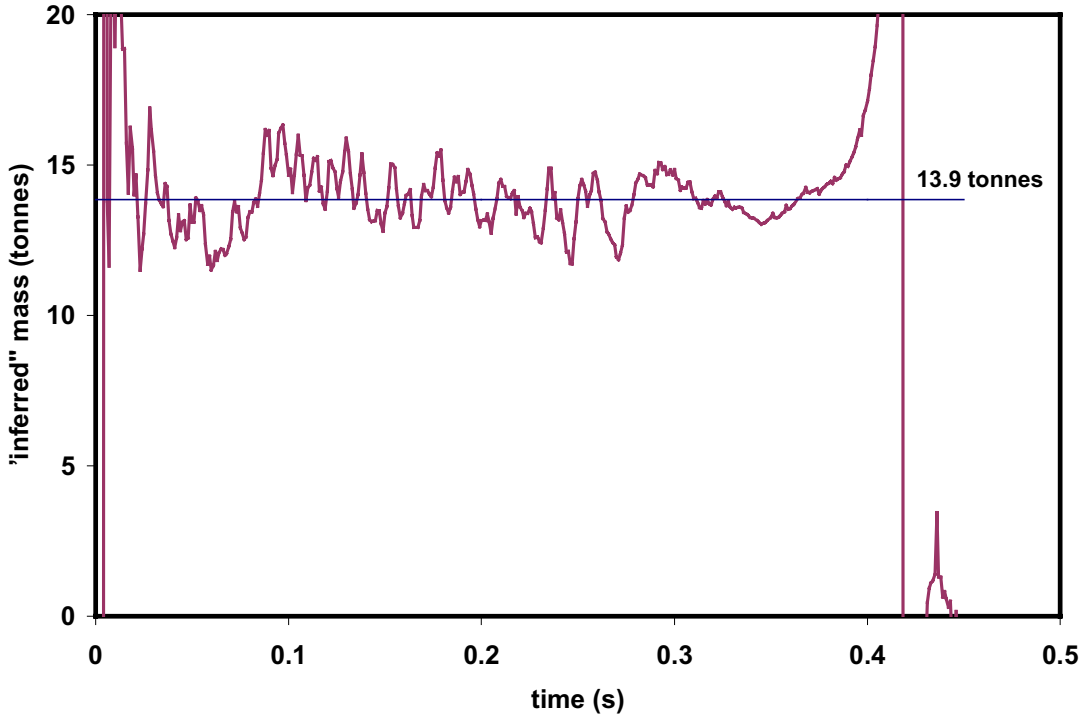

Figure 14 Inferred mass as a function of time for Test 20

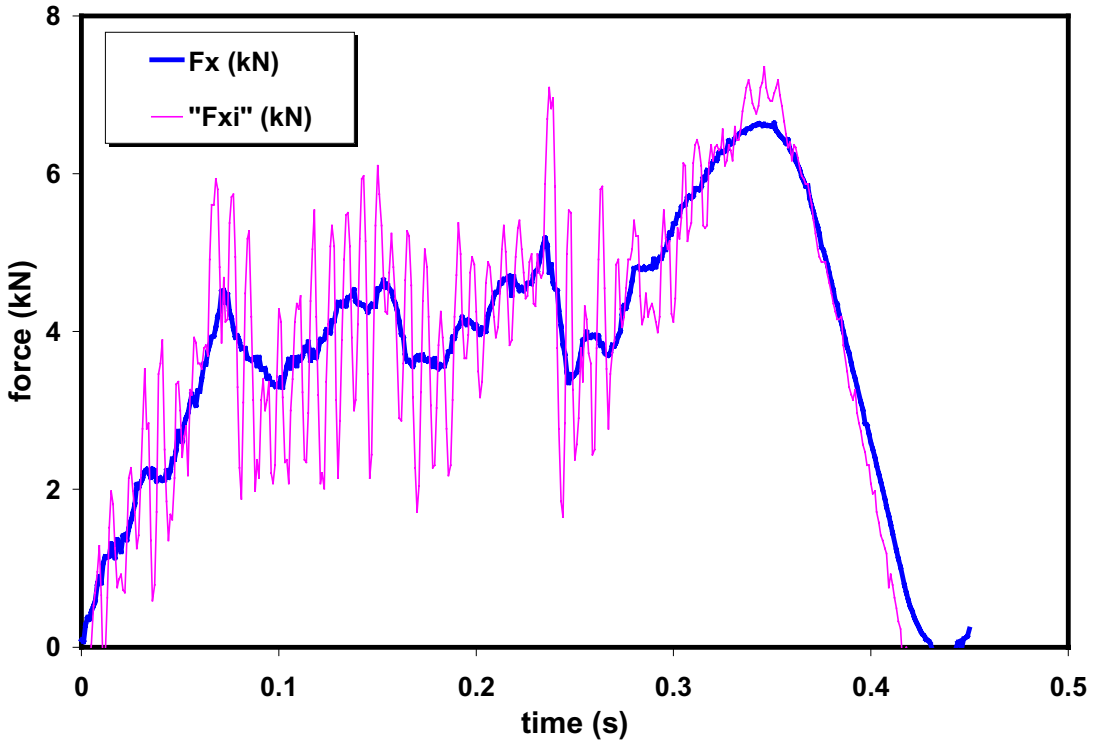

Figure 15 Measured impact force, Fx, and inferred force "Fxi," from acceleration in Test 20

Local pressures were also measured with pressure sensors installed in the test structure. From Figure 2 it can be seen that 12 sensors were installed in the face but that, because of the water level, only 8 had the possibility of responding to ice impacts. For Test 20 only a local ice pressure was seen by sensor PC6. The output of sensor PC6, together with F_x, is plotted in Figure 16. The maximum average pressure on the 12.5-mm diameter sensing face was about 0.5 MPa, and the maximum force was 6.6 kN. It can be seen that in the initial part of the impact the sensor was not in contact but, that as the impact proceeded beyond time 0.15 s, sensor PC6 began to respond to local ice pressures, and follows the trend of the force, F_x. Given the geometry of the ice edge (90^o wedge) and knowing the penetration of the test structure into the ice edge (integrating the velocity of Figure 13) and the ice edge thickness, in this case 150 mm, the nominal contact area between the ice and the structure can be determined. With this area and the measured force, F_x, average pressure over the contact face can be calculated. Figure 17 shows the calculated pressure versus area curve for this impact. The figure shows the descending pressure area characteristic which is typical of many impact scenarios (Frederking, 1998). The average pressure during the latter part of the impact is similar to that measured by the local pressure sensor, about 0.5 MPa.

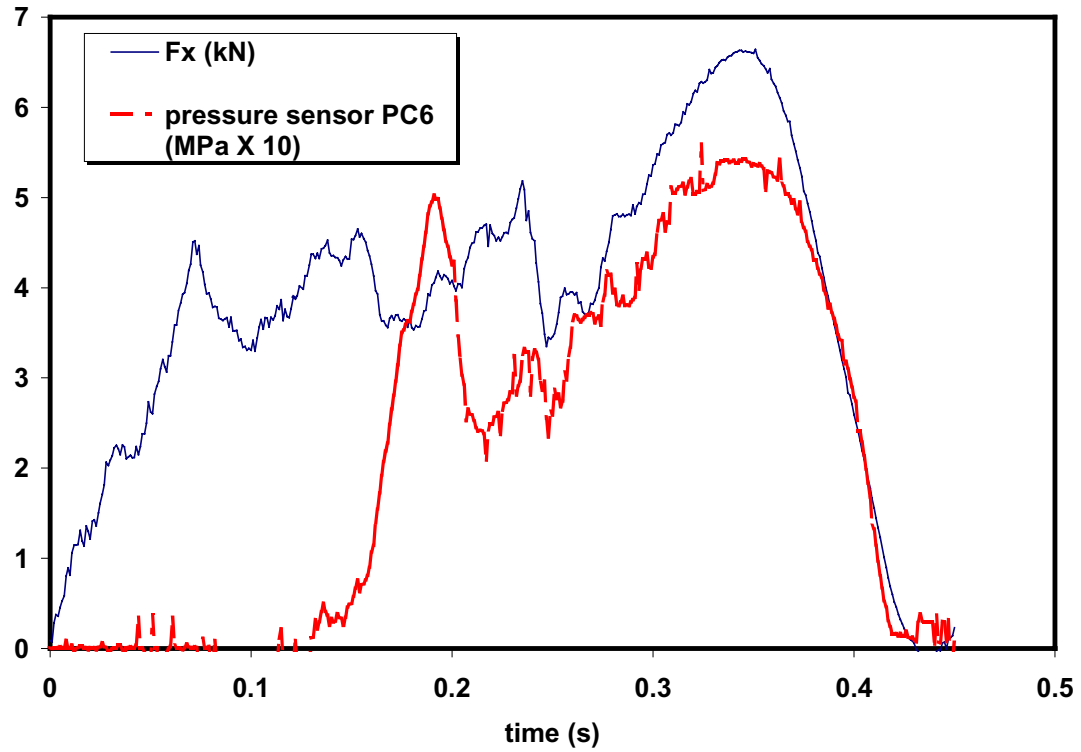

Figure 16 Comparison of impact force and local pressure on sensor PC6 for Test 20

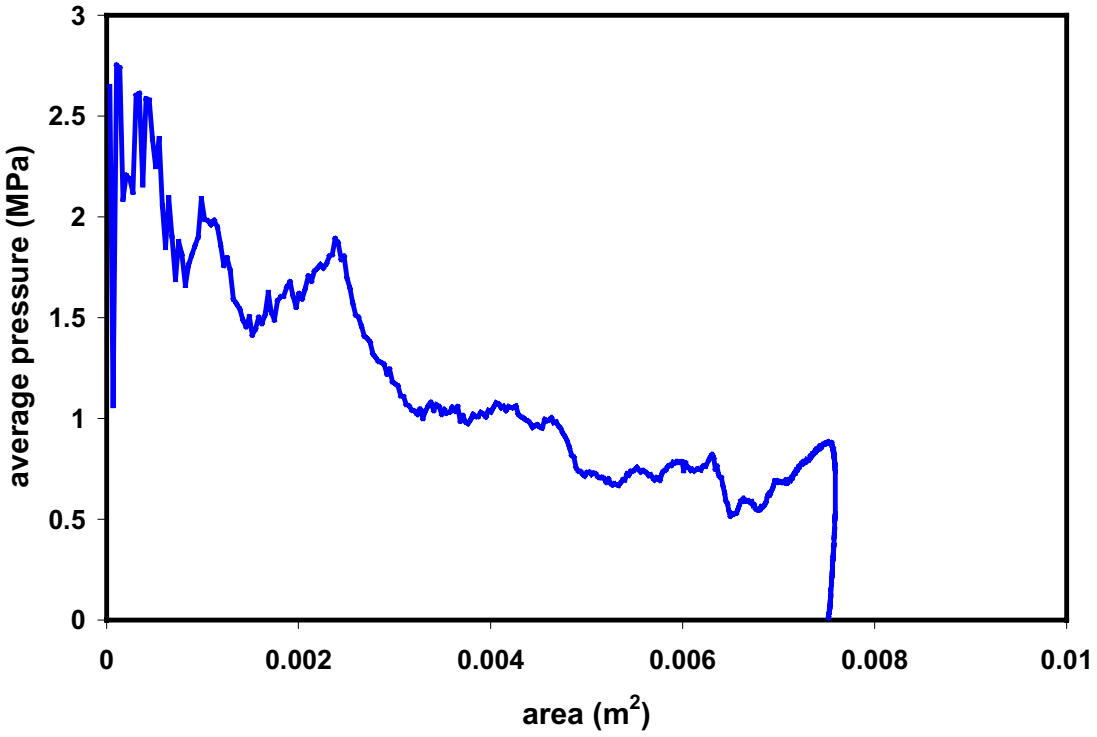

Figure 17 Pressure-area variation for Test 20

Figure 12 through Figure 17 demonstrate the detailed analysis that can be made for each test to describe ice impact failure characteristics and processes. Certain aspects of the detailed analysis will now be examined for all the tests.

4.2. Trends of Test Results

Table 2 is a compilation of all the test results. The first aspect of the results examined was the relation between the maximum force and the maximum acceleration. Plots for the three basic floe sizes are presented in Figure 18. A straight line is fit through the data of each group and the slope represents a mass of the floe. The floes masses inferred from the slopes of the curves are 13, 6.8 and 3.4 tonnes, as compared to 14.3, 7.8 and 4.1 tonnes calculated from the dimensions of the floes (see Table 1). The actual masses were smaller than the estimated masses, because the masses calculated from the dimensions of the ice floe assumed the thickness measured at the centre was uniform over the entire floe. However, the thickness of the ice was less around the edges and the floe was not perfectly rectangular.

Once the masses were known, the kinetic energy, KE, for each test was calculated using:

$$KE = \tfrac{1}{2}\, mV^2 \qquad (1)$$

where m is ice floe mass (including added mass) and V is ice floe impact velocity. The maximum force was plotted in Figure 19 as a function of kinetic energy, with separate symbols being used for each floe mass. A general trend of increasing impact force with increasing kinetic energy is observed; however, there is no significant difference between different floe masses, at least up to 50 Joules of kinetic energy. In spite of the large floe masses, kinetic energies are low because of the small impact velocities.

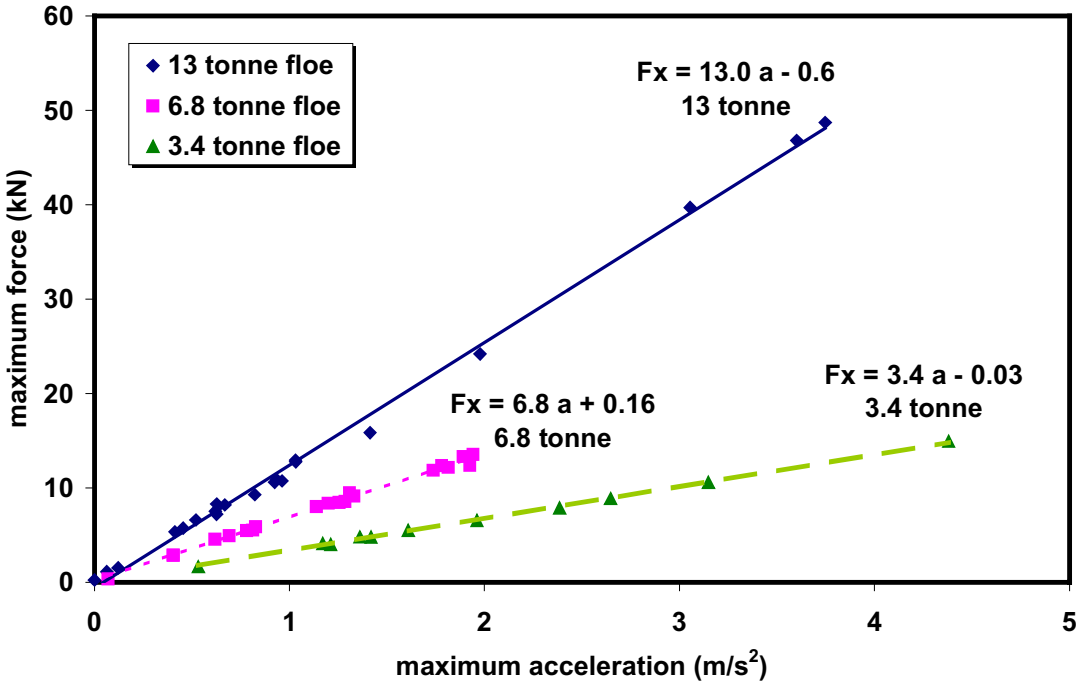

Figure 18 Maximum force as a function of maximum acceleration for the 3 sizes of ice floes.

The other factor that was investigated in this test series was the edge shape. Three basic shapes were used, a straight edge, a circular edge and a wedge shaped edge. The geometries of the edges are illustrated in Figure 6. All edge geometries were combined in Figure 19, but now the shapes will be separated. The greatest variety of shapes was explored for the 13-tonne floe impacts. Figure 20 presents the results for these tests. There is overlap in the results and it is difficult to discern any clear differences. Best fit lines from the origin have been fit through each set of results. Plots for the 6.8 t and 3.4 t floes are presented in Figure 21 and Figure 22, respectively. With the exception of the straight edge case, the 90° wedge appears to result in lower maximum impact forces for all three floes masses. The geometry of the wedge with its sharp tip is most likely responsible for the lower impact forces.

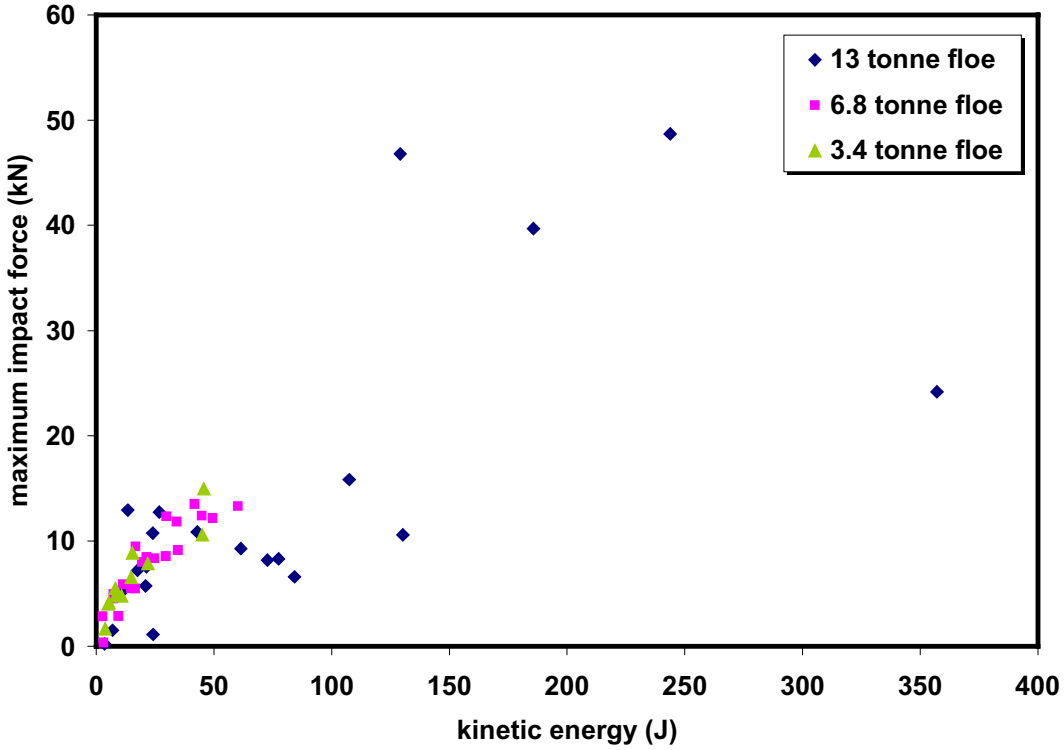

Figure 19 Maximum impact force as a function of kinetic energy.

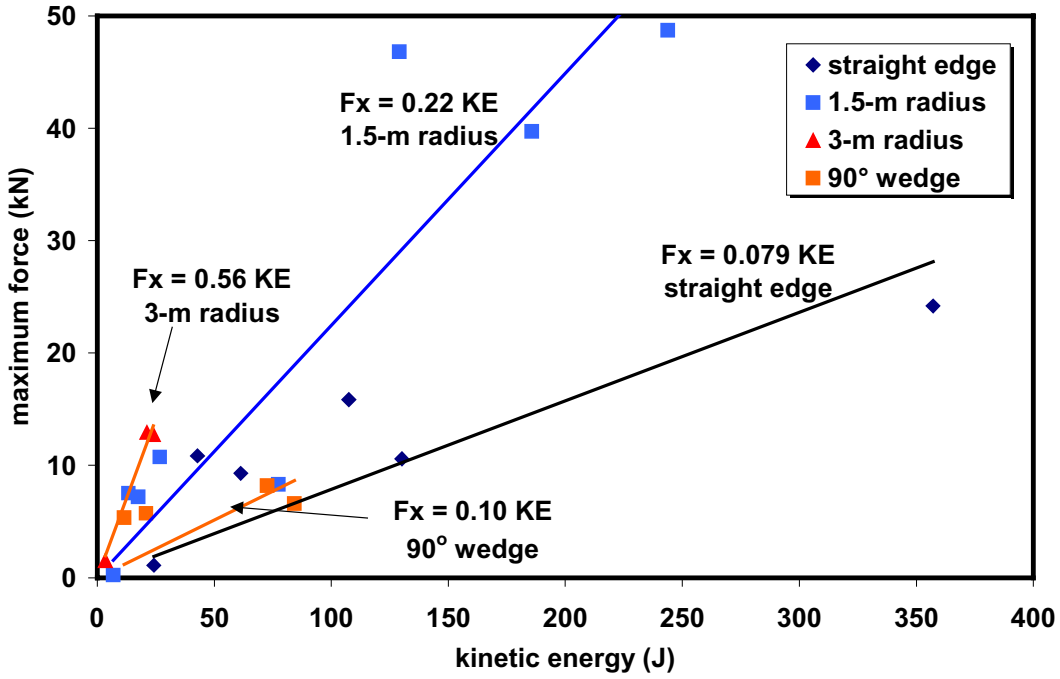

Figure 20 Maximum impact force as a function of kinetic energy for impacts of 13-t floe with various edge geometries

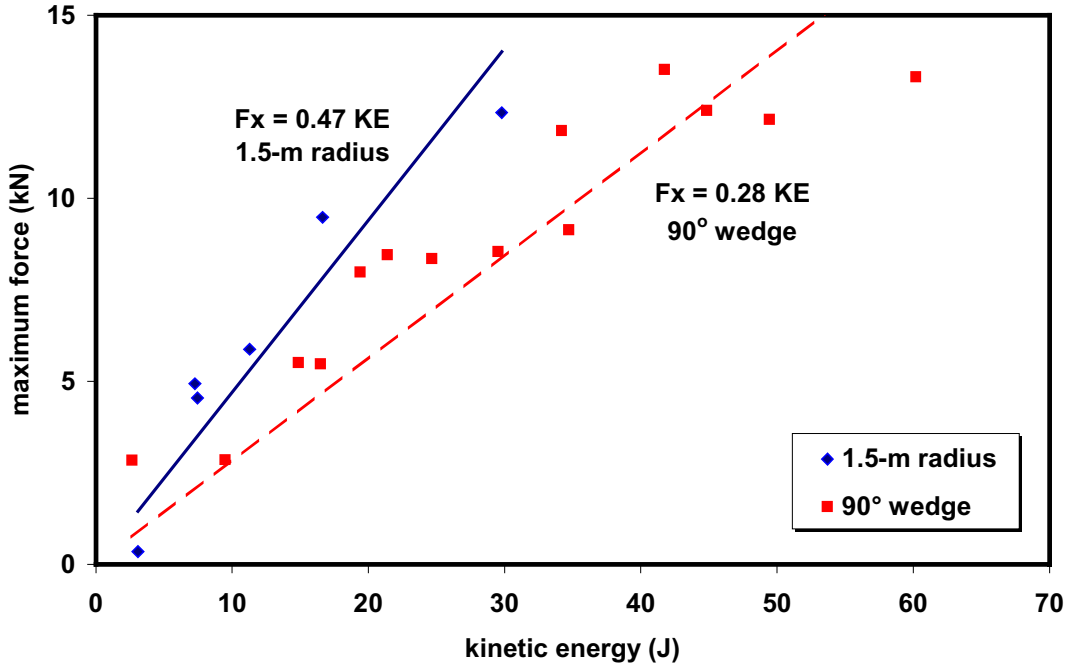

Figure 21 Maximum impact force as a function of kinetic energy for impacts of 6.8-t floe with various edge geometries.

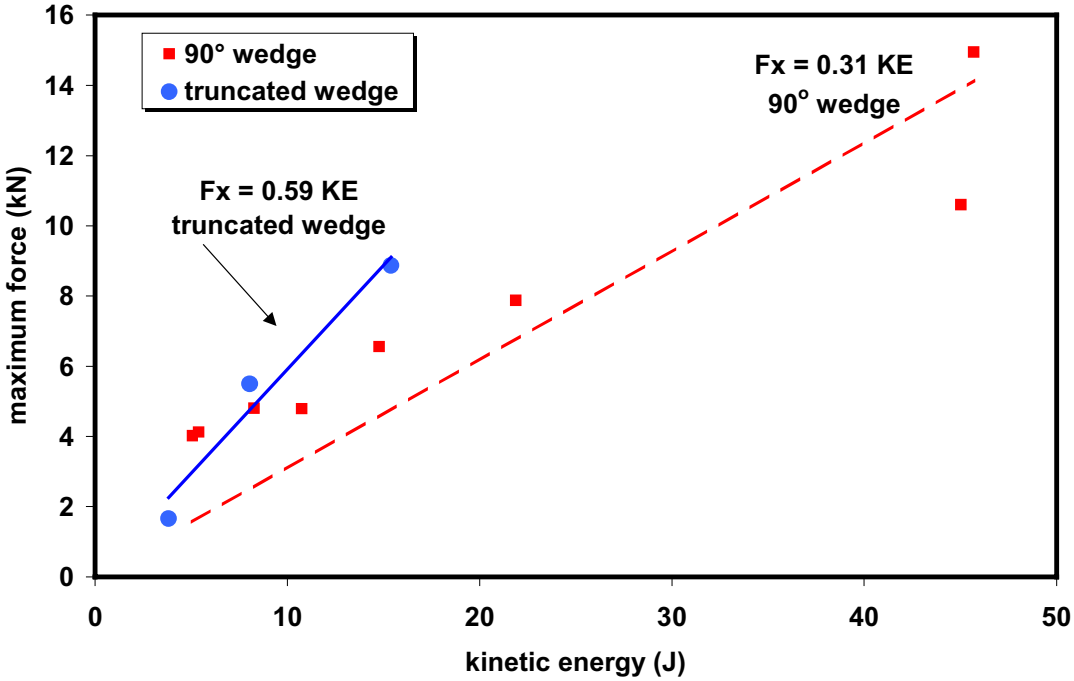

Figure 22 Maximum impact force as a function of kinetic energy for impacts of 3.4-t floe with various edge geometries.

It is also possible to make some predictions about maximum force as a function of kinetic energy. This can be done by assuming a constant crushing pressure, p_o, for the ice and conversion of all the kinetic energy to crushing of the ice. Two edge geometries will be considered, the 90° wedge and a 1.5-m radius. For the case of the 90° wedge the contact area A, is described by the following expression

$$A = 2\ h\ x \tag{2}$$

where h is ice edge thickness and x in the amount of penetration. The crushing force F, is given by

$$F = p_o\ A = p_o\ 2\ h\ x \tag{3}$$

The energy of ice crushing CE, is given by

$$CE = \int dx = \int p_o\ 2\ h\ x\ dx = p_o\ h\ x^2 \tag{4}$$

Equating crushing energy to kinetic energy KE

$$p_o\ h\ x^2 = KE \tag{5}$$

yields maximum extent of penetration

$$x = (KE/\ p_o\ h)^{1/2} \tag{6}$$

Substituting (6) into (3), the maximum impact force F_{max} is

$$F_{max} = p_o\ 2\ h\ (KE/\ p_o\ h)^{1/2} = 2(p_o\ h)^{1/2}\ (KE)^{1/2} \tag{7}$$

For the case of the 1.5-m radius the contact area A, is described by the following expression

$$\begin{aligned} A &= 2\ h\ (R^2 - (R - x)^2)^{1/2} \\ &\cong .\ 2\ h\ (2\ R\ x)^{1/2} \end{aligned} \tag{8}$$

where h is ice edge thickness and x in the amount of penetration. The crushing force F, is given by

$$F = p_o\ A = p_o\ 2\ h\ (2\ R\ x)^{1/2}\ . \tag{9}$$

The energy of ice crushing CE, is given by

$$\begin{aligned} CE &= \int F\ dx = \int p_o\ 2\ h\ (2\ R\ x)^{1/2}\ dx = 2\ p_o\ h\ (2\ R)^{1/2} \int x^{1/2}\ dx \\ &= 2\ p_o\ h\ (2\ R)^{1/2}\ 2\ x^{3/2}/3\ . \end{aligned} \tag{10}$$

Equating crushing energy to kinetic energy KE

$$(4/3)\, p_o\, h\, (2\, R)^{1/2}\, x^{3/2} = KE \qquad (11)$$

yields maximum depth of penetration

$$x = \{KE/\, (4/3)\, p_o\, h\, (2\, R)^{1/2}\, \}^{2/3}\, . \qquad (12)$$

Substituting (12) into (9), the maximum impact force F_{max} is

$$\begin{aligned} F_{max} &= 2\, p_o\, h\, (2\, R)^{1/2} \{KE/\, (4/3)\, p_o\, h\, (2\, R)^{1/2}\, \}^{1/3} \\ &= 2\, p_o\, h\, (2\, R)^{1/2} \{1/\, (4/3)\, p_o\, h\, (2\, R)^{1/2}\, \}^{1/3}\, (KE)^{1/3} \\ &= 2\, (3/4)^{1/3}\, (p_o\, h)^{2/3}\, (2\, R)^{1/3}\, (KE)^{1/3} \end{aligned} \qquad (13)$$

Figure 23 combines the measured data for the 13-t floe impacts with maximum impact load predictions using Equations (7) and (13). A constant crushing stress of 2000 kPa and an edge thickness of 150 mm were used in the calculations. As expected, the circular edge results in higher predicted impact loads.

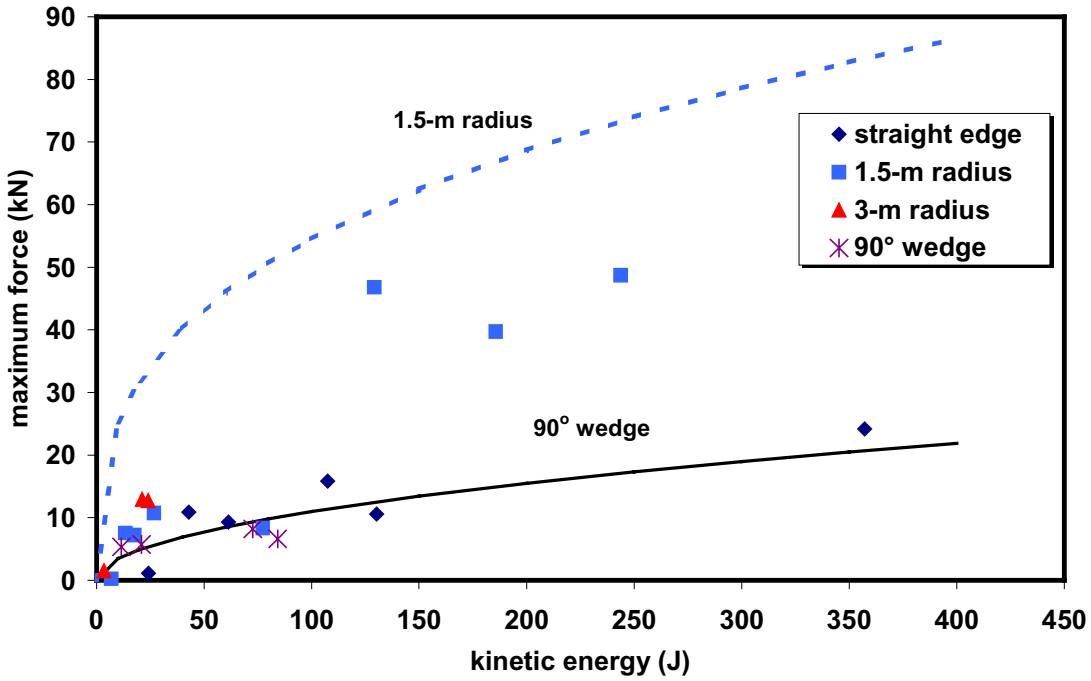

Figure 23 Predicted maximum impact force as a function of kinetic energy and comparisons of data from 13-t floe impacts.

4.3. Local Pressures

Local pressures were measured in all tests and time series plots are presented in Appendix A. No local pressures were registered in almost half the tests. This was due to a combination of small contact areas and the contact area not coinciding with the location of any of the sensors. The highest local pressure was measured in Test 36 and was 1.8 MPa on pressure sensor PC6. None of the other sensors registered any pressure in this test so it is reasonable to assume that the contact area was relatively small. In contrast, Test 39 had a maximum pressure of 1 MPa on Sensor PC6 plus two other sensors with simultaneous, but lower pressures. In other tests, Test 34 for example, the movement of local pressure from one sensor (PC7) to another (PC6) can be seen. The local pressure sensors provide details on the nature of each individual impact. The data can be used for analysis of the impact process.

5. SUMMARY AND CONCLUSIONS

The results of 52 impact tests with ice floes of varying shapes and sizes have produced a substantial body of data on impact forces, floe accelerations and local pressures. The combination of floe acceleration and independent impact force measurement is a unique data set, which also provides a means of determining the actual floe mass.

Three floe sizes were tested, 13 t, 6.8 t and 3.4 t, and impact velocities ranged from 23 mm/s to 234 mm/s. Three basic edge geometries were used, a 90^o wedge, 3- and 1.5-m radius and a straight edge. The maximum impact force measured was 50 kN for a kinetic energy of about 250 J. The maximum local ice pressure measured with the ice pressure sensors on the contact interface was 1.8 MPa.

An analysis of the maximum impact force as a function of kinetic energy indicated that it is a function of the kinetic energy raised to the $^1/_2$ or $^1/_3$ power, depending on the ice edge geometry. The measured impact forces qualitatively supported the analysis.

6. ACKNOWLEDGEMENTS

The authors would like to thank Ivana Skabova for assistance in preparing the plots in Appendix A; Michelle Johnston for preparing the thin sections and providing salinity measurements; and Wayne Jamieson for analyzing the videos to calculate impact velocities.

7. REFERENCES

Frederking, R. 1998. The Pressure-Area Relation in the Definition of Ice Forces, 8th International Offshore and Polar Engineering Conference, May 24-29, 1998, Montreal, Vol. II, pp. 431-437.

Frederking, R. and Sayed, M. 1989. Measurements of Ice Impact Forces on a Vertically Faced Bridge Pier. Proceedings OMAE'89, pp. 319-322, The Hague, Netherlands.

Haynes, F.D. at al. 1991. Ice Force Measurements on a Bridge Pier in the St. Regis River, New York. CRREL Special Report SR91-14, 6 pages, Hanover, NH, USA.

Michel, B., Ramseier, R. 1971. Classification of River and Lake Ice, Canadian Geotechnical Journal, Vol. 7, No. 1, pp.38-45.

Pratte, B.D., Timco, G.W. 1981. A New Model Basin for the Testing of Ice-Structure Interactions. Proceedings of the Sixth International Conference on Port and Ocean Engineering under Arctic Conditions, POAC'81, Volume II, pp 857 – 866, Quebec, Canada.

Wright, B.D. et al. 1998. Moored Vessel Stationkeeping in Grand Banks Pack Ice Conditions. Report prepared for the National Research Council of Canada, Report PERD/CHC 26-189.

Appendix A

Time Series of Test Data